Supporting Information

Size-selective Particle Trapping in Dielectrophoretic Corral traps

Tae Joon Kwak[1,†], Hwangjae Lee,[2,‡], Sang Woo Lee[3], Jörg C. Woehl[4,], Woo-Jin Chang[5,6,]**

[1] Center for Systems Biology, Massachusetts General Hospital, Boston, MA 02114, United States

[2] Department of Mechanical Engineering, KAIST, Daejeon 34141, Republic of Korea

[3] Department of Biomedical Engineering, Yonsei University, Wonju 26493, Republic of Korea

[4] Department of Chemistry and Biochemistry, University of Wisconsin-Milwaukee, Milwaukee, WI 53211, United States

[5] Department of Mechanical Engineering, University of Wisconsin-Milwaukee, Milwaukee, WI 53211, United States

[6] School of Freshwater Sciences, University of Wisconsin-Milwaukee, Milwaukee, WI 53204, United States

† This study was mostly done while T.J.K. was working at University of Wisconsin-Milwaukee.

‡ This study was mostly done while H.L. was working at University of Wisconsin-Milwaukee.

*Jörg C. Woehl: woehl@uwm.edu. Woo-Jin Chang: wjchang@uwm.edu

Table of Contents

Supplementary Figures

Supplementary Movie Descriptions

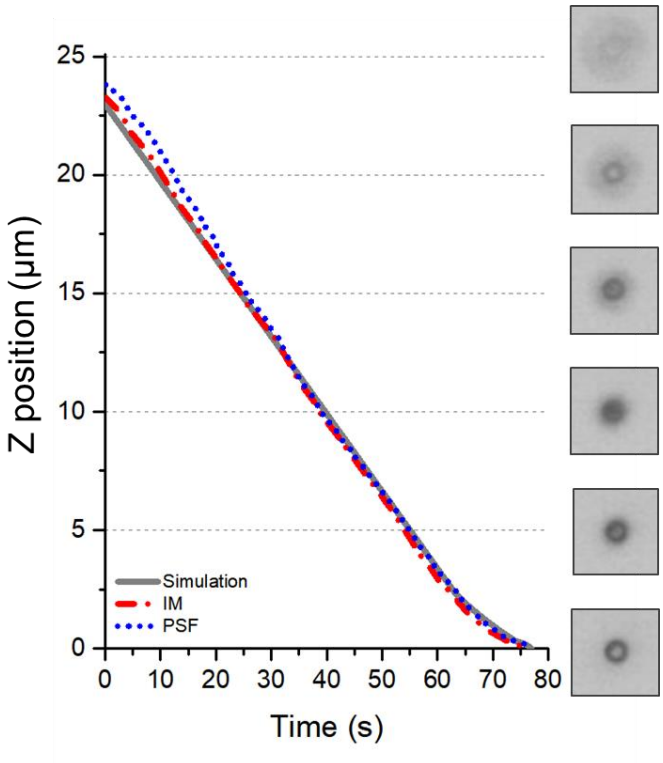

Figure S1. Comparison of IM and PSF methods for the determination of *z* particle positions. Both methods were applied to images of sinking 2 µm radius particles recorded at 5 frames per second using a high-speed camera (red and blue curves, respectively). Both methods yield very similar results and match closely the numerically simulated time-dependent sedimentation dynamics of a 2 µm radius particle (gray curve). The images to the right show representative experimental particle images at the corresponding *z* positions.

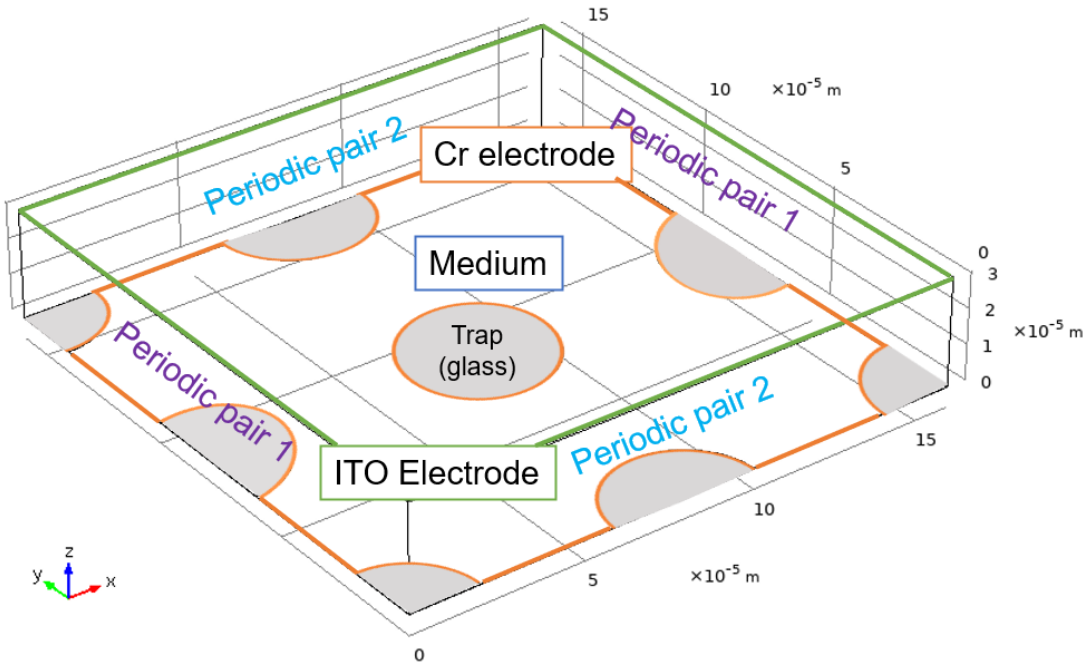

Figure S2. Boundary conditions and computational domain of the model of the microfluidic corral trap for finite element analysis. + V_{rms} and - V_{rms} were applied to the Cr electrode and ITO counter electrode respectively, and no electrical potential was applied to the circular trap area.

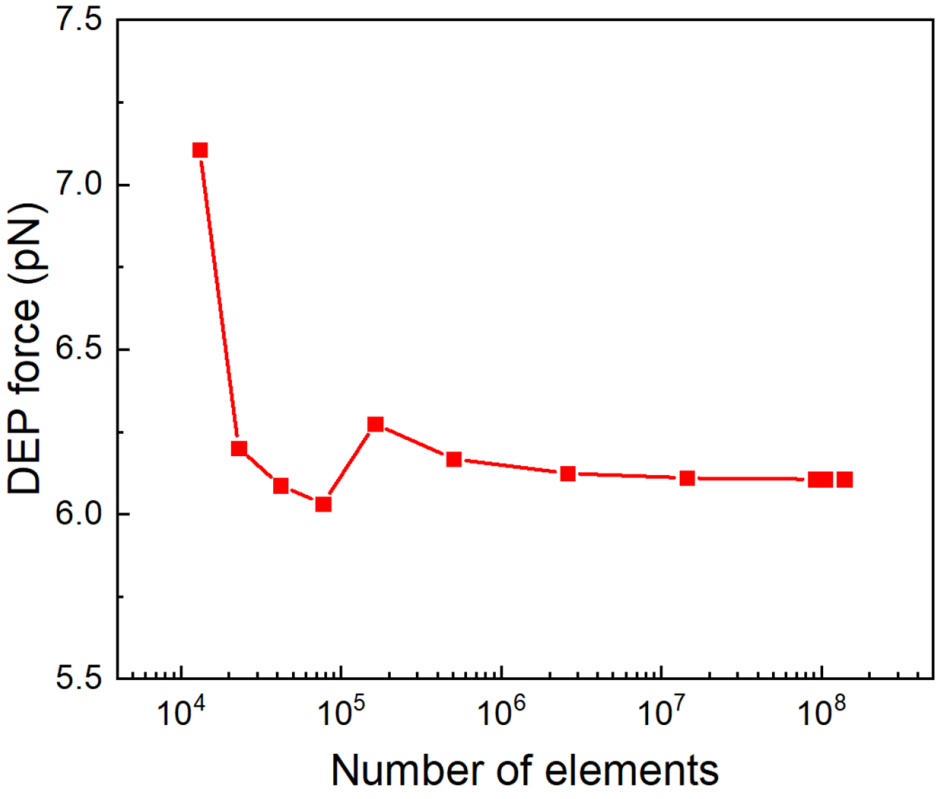

Figure S3. Mesh convergence test for numerical simulation. Refining mesh quality convergence test for DEP forces on a 2 μm microparticle in the center of the trap when 1 MHz 8 Vp-p AC is applied to the electrodes.

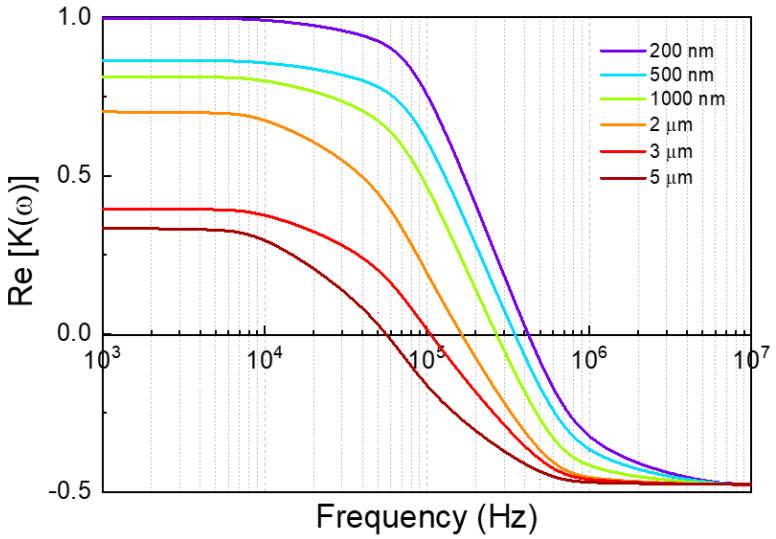

Particle size (nm)	200	500	1000	2000	3000	5000
Crossover frequency (Hz)	4×10^5	3.25×10^5	2.25×10^5	1.35×10^5	1×10^5	7×10^4
Particle conductivity (S/m)	2.5×10^{-3}	2×10^{-3}	1.4×10^{-3}	8.07×10^{-4}	5.93×10^{-4}	4.37×10^{-4}
Relative permittivity of the particle	2.5					
Medium conductivity (S/m)	2×10^{-4}					
Relative permittivity of the medium	80					

Figure S4. Calculated frequency dependence of the real part of the Clausius-Mossotti factor *K(ω)* for different particle sizes. The table lists the numerical values for physical and electrical properties of particles and medium used to obtain this plot and to calculate the dielectrophoretic forces experienced by particles interacting with DEP corral traps. The conductivity of the final solutions, obtained by dilution of the microparticle stock solutions with DI water, was 2 μS/cm. Particle conductivities were determined from experimentally measured cross-over frequencies.

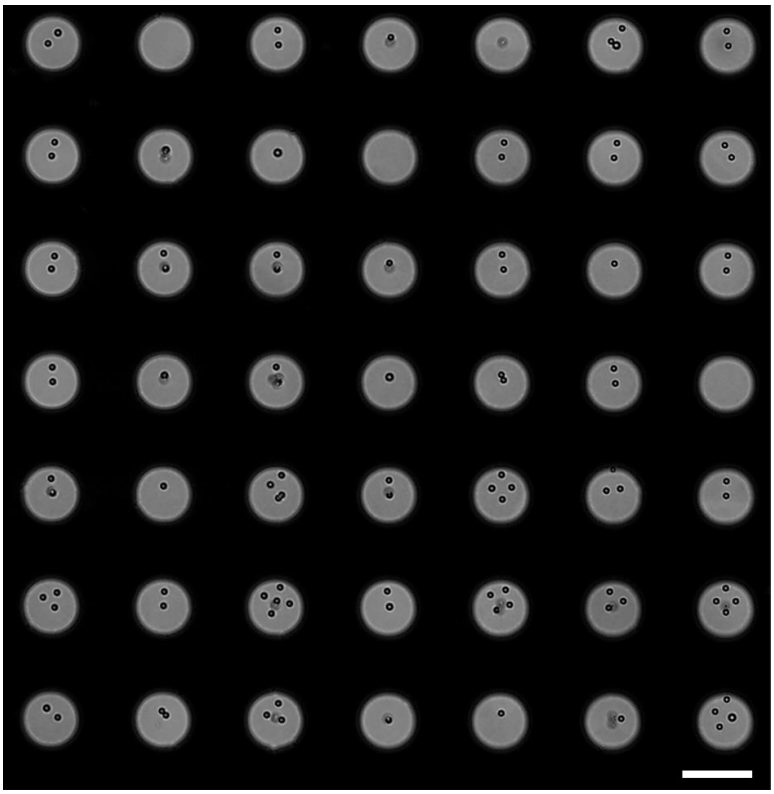

Figure S5. Size-selective multi-particle trapping. Multiple 2 μm radius polystyrene particles are captured in 40 μm diameter corral traps by applying 1 MHz 8 V_{p-p} AC to the electrodes while a mixture of 1 μm, 2 μm, and 3 μm radius particles is passing through the device over an extended period of time (microchannel height: 30 μm; linear flow velocity: 320 μm/s). Scale bar = 50 μm.

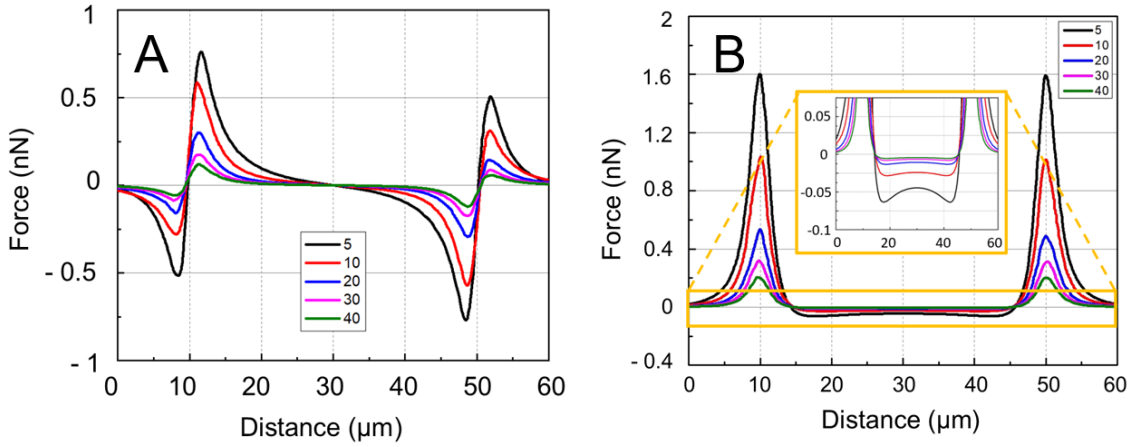

Figure S6. Comparison of DEP forces for different channel heights. (A) Simulated *x* DEP force components and (B) *z* DEP force components acting on a 2 μm radius polystyrene particle that moves in a straight line at z = 2 μm in the +*x* direction across the center of a 40 μm diameter corral trap when 1 MHz 8 $V_{p\text{-}p}$ AC is applied to the electrodes (microchannel heights: 5 μm, 10 μm, 20 μm, 30 μm, and 40 μm, respectively). Positive values indicate that the force points in the positive axis direction, and vice-versa. The *x* and *z* force components are stronger at lower channel heights. The insert in (B) shows a zoom of the section outlined in yellow; the trap center is located at 30 μm.

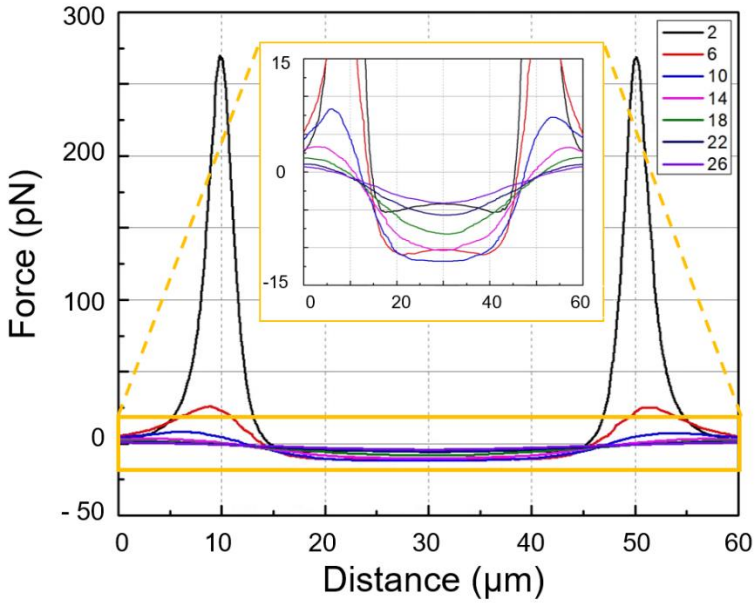

Figure S7. *Z* position dependence of the DEP force. The plot shows simulated *z* DEP force components acting on a 2 μm radius particle that moves in a straight line at various distances from the corral trap surface (ranging from z = 2 μm to z = 26 μm) in the +*x* direction across the center of a 40 μm diameter corral trap when 1 MHz 8 $V_{p\text{-}p}$ AC is applied to the electrodes (microchannel height: 30 μm). Positive values indicate that the force points in the positive axis direction, and vice-versa. The insert shows a zoom of the section outlined in yellow; the trap center is located at 30 μm.

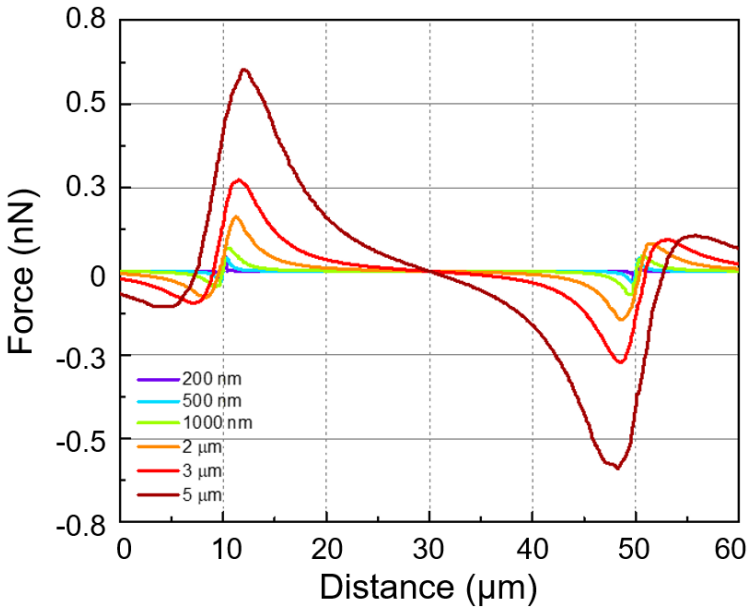

Figure S8. Comparison of DEP forces acting on various size particles. The plot shows simulated *x* DEP force components acting on a 200 nm, 500 nm, 1000 nm, 2 μm, 3 μm, and 5 μm radii particles that move in a straight line at z = 2 μm in the +*x* direction across the center of a 40 μm diameter corral trap when 1 MHz 8 $V_{p\text{-}p}$ AC is applied to the electrodes (microchannel height: 30 μm). Positive values indicate that the force points in the positive axis direction, and vice-versa. The trap center is located at 30 μm.

Movie S1. Flow controlled, size-selective trapping of 2 μm and 3 μm radius particles. At a linear flow velocity of 320 μm/s, 2 μm radius particles were selectively trapped in 40 μm diameter corral traps when 1 MHz 8 V_{p-p} AC was applied to the electrodes (0:01-0:30; microchannel height: 30 μm). When the voltage was turned off, the trapped 2 μm particles were removed with the flow (0:31-0:33). By increasing the flow rate to 590 μm/s, 3 μm radius particles were selectively trapped under otherwise identical conditions (0:34-1:18). When the voltage was turned off, the trapped 3 μm particles were removed with the flow (1:19-1:21).